# Under-Water Explosion Measurements from Small Charges at Short Ranges

A. H. Bebb

| | |
|---|---|
| **Email alerting service** | Receive free email alerts when new articles cite this article - sign up in the box at the top right-hand corner of the article or click **here** |

[ 153 ]

# UNDER-WATER EXPLOSION MEASUREMENTS FROM SMALL CHARGES AT SHORT RANGES

By A. H. BEBB

*Royal Naval Scientific Service*

Experiments made to obtain pressure-time records of under-water explosion waves are described. The explosives used were cylindrical or spherical, and varied in mass between 2 oz. and $1\frac{1}{4}$ lb. Measurements were taken at the outside edge of the charge and at other distances up to 100 charge radii. The pressure-sensitive element employed was a tourmaline gauge, either $\frac{1}{2}$ or $\frac{1}{4}$ in. in diameter.

The shock-wave parameters, at close distances in particular, were found to depend on the shape of the explosive charge. Since the front part of the shock pulse travels faster than the rest, the profile of the pulse spreads as the range increases. The time-constant of the pulse is considerably smaller close to the charge than it is farther away. The results obtained demonstrate the importance of the afterflow energy-flux density relative to the primary shock-wave energy-flux density, especially near to the charge.

The results give general confirmation of theories developed in the United States and in the United Kingdom.

## CONTENTS

## 1. Introduction

The research work described in this paper was carried out in the period February 1947 to April 1948, but the apparatus used had been developed and designed previously.

Insulated miniature piezo-electric gauges of tourmaline were used in the water to receive the pressure-time pulses of the shock-waves resulting from the under-water explosions. The gauges were joined to a non-microphonic telcothene cable, so designed as not to develop a spurious signal from electrostatic charges set up in its dielectric material due to ambient pressure changes caused by the explosions. The cable was connected to a wide-band amplifier, the output from which was connected to one beam of a double-beam cathode-ray oscillo-graph. The other beam was generally used for recording the time base for the shock-wave pulses. The pulses and time trace were recorded on a high-speed drum camera.

The explosives used in this work were approximately cylindrical $1\frac{1}{4}$ lb. T.N.T. standard demolition charges, and spherical P.E. 3 A and P.E. 2 charges respectively, varying in mass between $\frac{1}{8}$ and 1 lb. The pressure-time pulses of the shock-waves were recorded over ranges between 100 and 1 charge radii, and an attempt was even made to measure the pressure inside a spherical charge when it was exploded under water.

## 2. Nature of an under-water explosion

When a solid explosive is detonated under water, a shock-wave is produced in the water exhibiting an instantaneous pressure rise followed by an approximately exponential decay. At the instant of detonation the solid explosive is converted into gas of the same size but at a very high temperature and pressure. Because of the high pressure, the gas expands (pro-ducing a flow of water radially) and continues to expand until its pressure becomes less than the hydrostatic pressure of the water. Ultimately the excess pressure in the water recompresses the gaseous product of the explosive until, at its minimum size, a second shock-wave is emitted. This is known as the first bubble pulse, as distinct from the initial or primary shock-wave pulse. This compression of the water and recompression of the gas bubble continues until either the gas vents to the surface of the water or all its energy is expended.

## 3. Object of experiments

The object of the work was to record the primary shock-wave pulses from under-water explosions, thereby measuring the pressure, momentum and energy associated with ex-plosive charges.

Theories have been advanced as to the magnitude of pressures close to charges exploded under water, and therefore the range of measurements has extended from 100 to 1 charge radii, particular attention having been paid to the region near the charge, which has not previously been studied experimentally.

Furthermore, examination has been made of the manner in which the large steep-fronted shock-wave pressures encountered vary with distance, because of the expected theoretical departure from the inverse-distance relationship for sound waves of low intensity.

Also, as indicated above, the energy from an explosive charge is not only that radiated acoustically in the shock-wave and therefore irreversible, but there is obviously reversible energy available which is connected with the outflow and inflow of water and associated

therefore with the formation of subsequent bubble pulses. Examination of the records shows that, close to the charge, the magnitude of the afterflow energy-flux density is of the same order as the energy-flux density of the primary shock-wave. This is also in accord with theory.

### 4. Apparatus used for the experimental work

The apparatus developed for this investigation has been described fully in Admiralty reports (Bebb & Bundy 1945; Bebb, Wallace, Pringle & Bundy 1946; Bebb, Wallace, Taylor, Bundy & Hendry 1947). U.S. reports also deal with some of the instrumentation problems involved (Lampson 1943; Greenfield & Shapiro 1944; Cole 1944). The following notes explain in outline how under-water explosion pulses are recorded.

#### Piezo-electric gauge

The principle used in measuring the pressure from an under-water explosion is that when a piezo-electric crystal is subjected to an applied force, an electric charge is developed on the crystal proportional to the force. A suitable crystal is tourmaline.

The gauges used for these measurements consist of two tourmaline disks $\frac{1}{16}$ in. thick, normally $\frac{1}{2}$ or $\frac{1}{4}$ in. in diameter. The faces of the disks are silvered and a silver electrode is located between the disks. By means of a special treatment in a muffle furnace at $550°$ C, the disks are fused together to form a gauge unit. The outer faces of the disks are soldered to the braid of the special telcothene cable by means of annealed copper ligaments, whereas the central silver electrode of the gauge unit is connected to the central conductor of the cable. Rubberoid wax is used to fill the air cavities in the base of the gauge unit and thus prevent reflexions being superimposed on the shock-wave pressure-time pulses. The gauge is insulated with latex. Figure 1 illustrates a gauge in process of construction.



FIGURE 1. Piezo-electric gauge before application of rubberoid wax and natural latex. Also after completion of curing process.

#### Cable and electrical circuit

The cable consists of a stranded central conductor, inserted in a telcothene insulator whose inner and outer surfaces are coated with graphite. The resistance of the outer graphited surface is not greater than 25,000 ohms/in. The outer graphited surface of the telcothene is gripped tightly by a wire braid conductor, and a second insulating sheath of telcothene surrounds the braid tightly also. A protective sheath of the highest grade rubber compound

lapped with cotton tape and a weatherproof wax compound finish surrounds the second telcothene layer. Figure 2 indicates the construction of the cable.
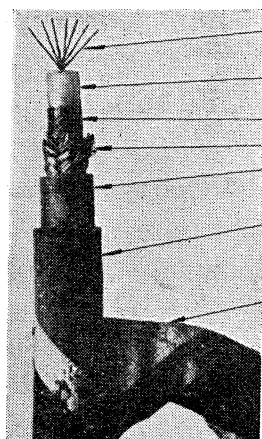


central conductors

telcothene
Aquadag or graphite
braid
outer telcothene covering

tough rubber sheath

canvas tape

FIGURE 2. Special cable for use with piezo-electric gauge.

The conductive graphited layers of this non-microphonic cable prevent unwanted electrical signals due to extraneous pressures being superimposed on the shock-wave pulses.

Unlike rubber-sheathed cables, the capacitance of this cable does not decrease with increase in frequency, and so the record of the under-water shock-wave pressure-time pulse does not give an overestimate in peak pressure and an underestimate in time-constant.

A resistance of 85 ohms—the surge impedance value of the cable—is inserted in series with the central core of the cable. To control the voltage input into the amplifier the cable is then shunted by a variable capacity of magnitude not less than five times the cable capacity. Previous work had shown that with these conditions fulfilled, damped oscillations reflected from either end of a long cable are suppressed and prevented from being superimposed on the pressure-time pulses.

*Amplifier*

The two-stage amplifier has a gain of about 500. It has a uniform response within 1 db. for frequencies ranging from 40 to 460,000 c./sec., and its output valve can handle an equivalent d.c. voltage of 200 V.

*Cathode-ray oscillograph and camera*

The 9 in. cathode-ray oscillograph is a double-beam type with 'floating plates'. The amplifier output, with a 150-megohm resistor across it, is connected directly to one plate of the oscillograph. The output from a standard beat frequency oscillator is connected to the second plate of the oscillograph to provide a 10 kc./sec. time base for the shock-wave records.

The camera consists essentially of a drum, two metres in circumference, grooved to carry 35 mm. film on its periphery. The drum is rotated by an electric motor, and a choice of gears give speeds varying between 3 and 30 m./sec., the highest speed being used in recording shock-wave pulses. A lens system, $f1\cdot9$ and focal length 10 cm., is used to focus the cathode-ray spots on to the film, giving an optical reduction of $2:1$.

*Gauge calibration*

The piezo-electric gauge is inserted into a reinforced cylindrical steel pressure pot filled with water and provided with a calibrated Bourdon gauge. By means of a pump, the piezo-electric gauge is subjected to hydrostatic pressure, and the pressure is released by cutting an annealed copper diaphragm. A similar method of calibrating gauges had been used by other workers (Wood & Lakey 1924).

## 5. EXPERIMENTAL ARRANGEMENTS

### Suspension of explosives and gauges

The under-water explosions were carried out in sea water of depth 36 ft., and free of tidal movements. The charges and gauges were hoisted from a boom and immersed to a depth of 12 ft.

When the pressure-time pulses for the T.N.T. charges were recorded the charge and gauge were suspended independently, but when the pulses for the P.E. charges were recorded, a more accurate arrangement was used whereby both charge and gauge were lowered together into the water on a mild steel ring. This latter method enabled distances between charge centre and gauge centre to be measured with considerable accuracy.

Records were also obtained simultaneously from two piezo-electric gauges spaced exactly 1 ft. apart on a rigid framework. By means of this arrangement the *mean* shock-wave velocity over this distance is determined, and its variation with the shock-wave peak pressure at the mid-point between gauges tabulated and graphed. The time base in this instance was provided by a standardized valve-maintained tuning fork (Munz 1945).

### Types of explosives

The explosives used were standard $1\frac{1}{4}$ lb. T.N.T. demolition charges fitted with primers and detonators. These are approximately cylindrical in shape, the length-diameter ratio being 2·45/1.

All P.E. charges were spherical, and these varied in mass between $\frac{1}{8}$ and 1 lb. No primers were used with these charges.

### Orientation of tourmaline gauges

To enable the pressure-time history at a point in the water to be measured, the tourmaline gauges should be infinitesimally small. But since the voltage injected into the amplifier depends upon the surface area of the tourmaline gauge, this sensitivity requirement gives an optimum limit to the size of gauge. Its thickness is also determined by practical considerations such as crystal robustness.

The gauge was always held edge-on to the charge, and because the shock-wave takes a finite time to traverse the gauge diameter, there is a tendency for the average pressure in the shock-wave rather than for its instantaneous peak pressure to be recorded. However, minor corrections have been applied to meet these limitations, and these are discussed later.

## 6. LIFE OF PIEZO-ELECTRIC GAUGES

The shock-wave peak pressures encountered in this work varied between 2,000 and 500,000 lb./in.$^2$, and the gauge mostly used was $\frac{1}{4}$ in. in diameter. About 100 shots were fired without

gauge failure for recorded pressures varying between 2,000 and 10,000 lb./in.², and about 20 shots for pressures ranging between 10,000 and 50,000 lb./in.². However, for pressures in excess of 50,000 lb./in.², one gauge per shot was required.

A complete pressure-time signature corresponding to a peak pressure of 135,000 lb./in.² was obtained, but for higher pressures, peak values only could be recorded.

### 7. The shock-wave pressure-time record

#### Mean shock-wave velocity

This is derived by measuring the time interval between shock-wave signatures obtained from two tourmaline gauges spaced 1 ft. apart. The *mean* shock-wave velocity was determined for changes in shock-wave pressures from approximately 1,000 to 20,000 lb./in.². In practice there are considerable difficulties in measuring the *mean* velocities for higher pressures, but as the limited results obtained are in reasonable agreement with theory, the theoretical results showing the relationship between *instantaneous* shock-wave velocities and shock-wave pressures were applied to correct the observed shock-wave pressures at varying ranges from the explosive.

#### Time-constant

The time-constant of the shock-wave was determined by measuring the time interval taken by the true peak pressure at zero time to fall to $1/e$ of its value, the peak pressure value being derived fairly rapidly by successive approximation.

At very short ranges of 1 or $1\frac{1}{2}$ charge radii, where only peak pressures could be measured, it was possible to estimate the time-constants without incurring much error by extending the practical curve of time-constant against range, bearing in mind the shape of the theoretical curve.

#### Peak pressure

Typical examples of pressure-time records are shown in figure 3. These show a sudden rise in pressure followed by a decay, approximately exponential in form. The true peak pressure is determined from the formula $p_0(1+a/\tau c)$, where $p_0$ is the measured or observed pressure in lb./in.², $a$, the piezo-electric gauge radius in feet, $\tau$ (sec.) the time-constant of the shock pulse (i.e. the time taken for the pressure to fall to $1/e$ of its true peak value) and $c$ (ft./sec.) the shock-wave velocity in water at the true peak pressure (Bebb & Bundy 1945; Bryant 1945; Arons & Smith 1946). Normally the correction is only of the order of 2 or 3 %.

#### Impulse of unit area

The impulse of unit area is given by $\int_0^T p\,dt$ lb./in.² sec., where $T$ sec. is the extent over which integration has been carried out.

To evaluate the area of the pressure-time shock-wave $\int p\,dt$, the records were enlarged about 14 times by means of a microfilm printer-viewer, the image of the enlarged record being produced on a transparent sheet of millimetre graph paper. In conformity with the peak pressure corrections, area corrections have been applied.

The ordinates of the pressure-time records were measured every 10 or 20 $\mu$sec. from zero time, $T = 0$ (i.e. the time when the shock wave reaches the centre of the gauge), to $T = 10\tau$.

Generally speaking, there is not much positive pressure at this time, and for ranges less than 5 charge radii there is certainly no measurable pressure. It is estimated that in limiting area measurements at $10\tau$, the error in impulse measurement may reach 5 %.

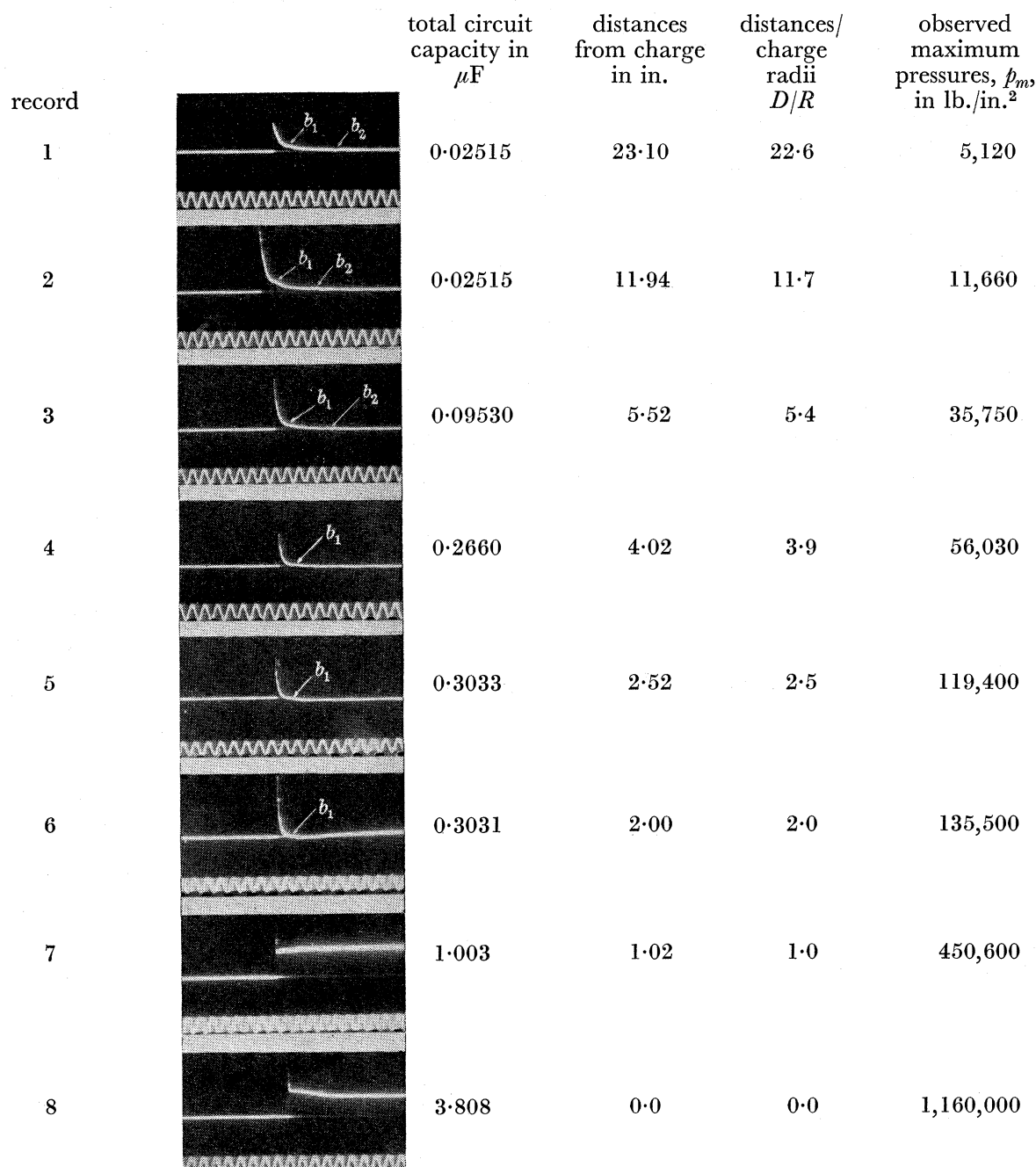| record | | total circuit capacity in $\mu$F | distances from charge in in. | distances/ charge radii $D/R$ | observed maximum pressures, $p_m$, in lb./in.$^2$ |
|---|---|---|---|---|---|
| 1 | | 0·02515 | 23·10 | 22·6 | 5,120 |
| 2 | | 0·02515 | 11·94 | 11·7 | 11,660 |
| 3 | | 0·09530 | 5·52 | 5·4 | 35,750 |
| 4 | | 0·2660 | 4·02 | 3·9 | 56,030 |
| 5 | | 0·3033 | 2·52 | 2·5 | 119,400 |
| 6 | | 0·3031 | 2·00 | 2·0 | 135,500 |
| 7 | | 1·003 | 1·02 | 1·0 | 450,600 |
| 8 | | 3·808 | 0·0 | 0·0 | 1,160,000 |

FIGURE 3. Typical pressure-time records from $\frac{1}{4}$ lb. P.E. 3A spherical charges with a $\frac{1}{4}$ in. diameter tourmaline gauge. (Time scale for records = 10,000 c./sec.)

*Energy-flux per unit area and total energy*

The total energy from an under-water explosion is the sum of the irreversible energy in the shock-wave together with the reversible or afterflow energy associated with the radial motion of the water surrounding the charge.

The irreversible energy-flux density is $(1/\rho_0 c_0)\int_0^T p^2\,dt$. But this formula for acoustic waves of small amplitudes has to be modified to deal with the high pressure shock-waves encountered in this work. This is dealt with in appendix 1, and the formula now becomes

$$(A_0/\rho_0 c_0)\int_0^T p^2\,dt.$$

The reversible energy-flux density is given by $(1/\rho_0 D)\int_0^T p\left(\int_0^t p\,dt\right)dt$ as shown in appendix 2.

The total energy, as shown in these appendices, is given by

$$E = (4\pi D^2)\left\{(A_0/\rho_0 c_0)\int_0^T p^2\,dt + (D/a\,.\,1/\rho_0 D)\int_0^T p\left(\int_0^t p\,dt\right)dt\right\},$$

where $a$ is the value of the explosion bubble radius at time $T$ (Taylor 1942; Comrie & Hartley 1942). Expressed in appropriate units, the total energy becomes

$$E = (10{,}475\,.\,4\pi D^2)\left\{(A_0/c_0)\int_0^T p^2\,dt + (D/a\,.\,1/D)\int_0^T p\left(\int_0^t p\,dt\right)dt\right\}\text{ft.lb.}$$

The measured value $1\cdot021$ g./cm.$^3$ has been substituted for $\rho_0$. In this expression the pressure $p$ is expressed in lb./in.$^2$, the distance $D$ from the charge in feet, the bubble radius $a$ in feet at time $T$ sec., and the *sound*-wave velocity $c_0$ in ft./sec. at the corresponding sea-water temperature.

The values of the areas denoted by the above two integrals were again evaluated to time $10\tau$ from the already measured ordinates. Since the irreversible energy is proportional to the squares of the pressures, the error in not extending the integral beyond $10\tau$ is negligible. But from appendix 3, as the reversible afterflow energy is proportional to the square of the impulse, the error in not extending integration may amount to some $10\%$.

## 8. Results

### Records: some theoretical considerations

Reference is made mainly to the eight selected under-water explosion pressure-time records from $\frac{1}{4}$ lb. P.E. 3 A charges at various ranges, shown in figure 3. The peak pressures of these particular records vary from about $5{,}100$ lb./in.$^2$ at a range of 23 charge radii to $450{,}000$ lb./in.$^2$ at 1 charge radius. No complete pressure-time record was obtained for a range less than 2 charge radii ($135{,}000$ lb./in.$^2$) because of gauge failure.

Two attempts were even made to measure the pressure inside the charge as it was detonated, by inserting the gauge centrally in it. One of these is shown in record 8 of figure 3, and the peak value measured was of the order of $1{,}200{,}000$ lb./in.$^2$. However, as negative pressures of this order appeared on the original records to precede these peak pressures by about a microsecond or so, it is probable that the gauge had been damaged, and that the values obtained are unreliable. No use was made therefore of record 8, figure 3 in the analysis.

As the range is lessened, careful measurement reveals that the time of rise of the pressure-time wave becomes less also, due to increase in shock-wave speed across the gauge diameter.

The records show that the profile of the pressure-time wave spreads with propagation, and therefore the duration and time-constant increases with increase in range. This results from the fact that the velocity of propagation of the shock-wave depends upon its pressure

amplitude and the large-amplitude front part of the wave travelling faster than its rear, forces the wave to spread. This is largely confirmed by the work of other experimenters except in cases where the charges have been too small to make measurements reliable (Arons & Smith 1946; Coles, Christian, Slifko, Niffenegger & Rogers 1946; Osborne & Taylor 1944, 1946; Cole & Coles 1947). The results are in accord also with theory (Kirkwood & Bethe 1942; Cole 1948; Osborne & Taylor 1944, 1946; Cole & Coles 1947; Kirkwood & Montroll 1942; Kirkwood & Richardson 1942; Kirkwood, Montroll & Richardson 1942; Kirkwood, Brinkley & Richardson 1943; Kirkwood & Brinkley 1944, 1945).

At close ranges of about 5 charge radii and less, illustrated, for example, in records 3 and 4 of figure 3, negative pressures are discernible which begin at 0·5 and 0·2 msec. after the onset of the shock wave and reach peak values of 450 and 1,540 lb./in.$^2$ respectively. These records are referred to in particular because the gauges survived the firing of the shots. This early unsustained negative pressure is, however, not to be confused with the later fall of pressure in the gas bubble below the hydrostatic pressure of the water which is always manifest in records which extend to show bubble pulses. It is considered that at very close ranges the ionized gaseous product of the explosive tends to envelop the gauge, and the negative-pressure readings are probably associated with this phenomenon.

Irregularities or bumps $b_1$, $b_2$ are marked on the records of figure 3. Since $t_1/M^{\frac{1}{3}}$, where $t_1$ is the time from the onset of the shock wave to the bump $b_1$ and $M$ is the mass of the explosive, was found to be constant at $210 \times 10^{-6}$ sec./(lb.)$^{\frac{1}{3}}$ for all P.E. 3 A charges, it is concluded that bump $b_1$ is a property of the shock wave, and is due probably to internal reflexions in the expanding bubble consequent upon the detonation wave reaching the charge surface. This is in agreement with the results of other workers in this field (Arons & Smith 1946; Cole 1948; Coles et al. 1946; Kennard 1941; O.S.R.D. 4874, 1945).

The calculations of Temperley & Craig (1945) enable the details of this process to be filled in. What seems to happen is that a rarefaction wave travels in to the gas from the surface. This is reflected at the centre, travels back about half-way to the interface and then turns into an inwardly going shock-wave. This is again reflected at the centre and travels out as a shock, eventually overtaking the interface and affecting the water.

The time $t_2$ from the onset of the shock-wave to bump $b_2$ has been proved to be directly dependent upon the distance of the gauge from its supporting ring, and these bumps are therefore reflexion pulses from the supporting mild steel ring. Other oscillations on the steep rise of the pressure-time wave are probably due to natural oscillations set up in the gauge crystals, whereas small oscillations as the pressure wave begins to decay are probably reflexions from the fairly abrupt join of the gauge to the cable.

The profile of shock-wave records for approximately cylindrical T.N.T. charges were observed to be more irregular than those for spherical P.E. 2 charges. This is probably because of interference of pressure fronts from different parts of the T.N.T. charge, and also because of internal reflexions resulting from the detonation wave reaching the charge surface.

*Tables: mean standard deviations*

The tables of results are not included in this paper, but graphical illustrations of all the results are given in full. To give an indication of the scatter of observations around the mean, the values of the coefficient of variation of observations were determined.

162          A. H. BEBB

The mean standard deviations from the tables for time-constants, peak pressures, impulses, primary energies, afterflow energies, and shock-wave velocities are 4·8, 2·7, 4·3, 5·0, 8·8 and 0·5 % respectively (Yule & Kendall 1945).

The final results in the formulae derived in §9 are correct to three significant figures.

## 9. Discussion of results. Comparison with theory

### Graphs

The experimental data given in the tables have been graphed in figures 4 to 17.

Whilst it would have been quite possible to relate the various shock-wave parameters with range by complex equations without any particular physical significance, the more practical step was taken of using the method of least squares to derive power-law equations to fit the observed points (Yule & Kendall 1945).
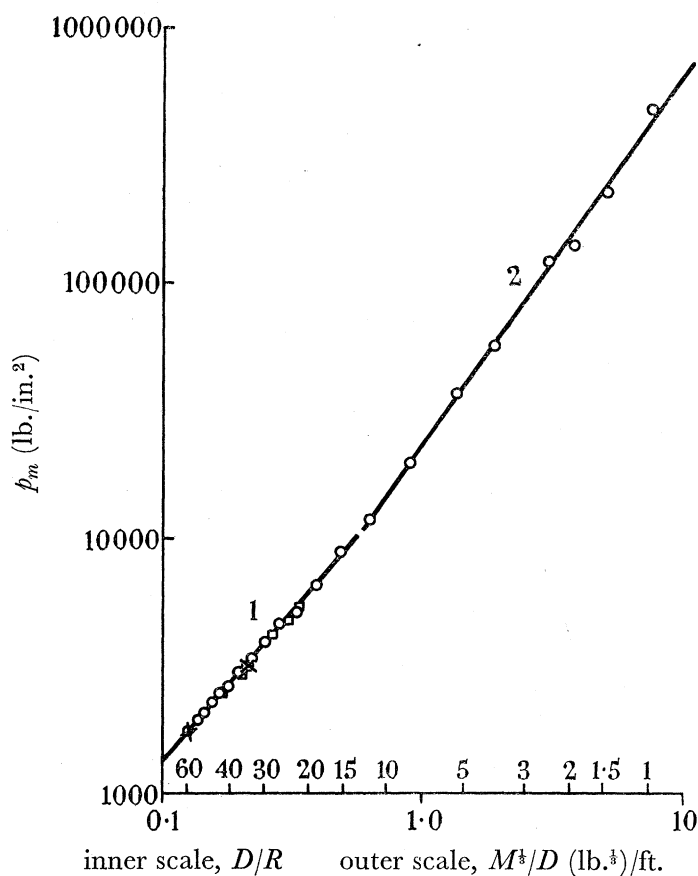


Figure 4. Maximum pressure against $M^{\frac{1}{3}}/D$ and $D/R$, for spherical P.E. charges.
Curve 1, $p_m = 19,400(M^{\frac{1}{3}}/D)^{1·15}$; curve 2, $p_m = 22,400(M^{\frac{1}{3}}/D)^{1·45}$.
○ $\frac{1}{4}$ lb. P.E. 3A, $\frac{1}{4}$ in. dia. gauge;     × $\frac{1}{4}$ lb. P.E. 2, $\frac{1}{4}$ in. dia. gauge;
□ $\frac{1}{8}$ to 1 lb. P.E. 3A, $\frac{1}{4}$ in. dia. gauge;   △ 1 lb. P.E. 2, $\frac{1}{2}$ in. dia. gauge.

### Maximum pressures and the function $p_m D/R$

Figure 4 shows how peak pressures for spherical P.E. charges vary with ranges from 60 to 1 charge radii. Within this range the large pressures encountered with under-water shock-waves do not vary inversely with distance as do small-amplitude sound waves, and this

becomes noticeable at closer ranges than say 13 charge radii where the pressure varies inversely as distance to the power of 1·5 approximately. This digression from the acoustic law is well illustrated at near ranges in figure 5, where the plotted points of $p_m D/R$ do not lie on a straight line parallel to the abscissa. The theoretical curves of Temperley & Craig (1945) and of Kirkwood & Brinkley (1944) are drawn on figure 5 also, for comparison, although these curves are actually applicable to spherical T.N.T. charges. The parameters of the Kirkwood-Brinkley theory were obtained from and made to fit existing U.S. data at the longer ranges. Very near the charge, the observed peak pressures are even lower than the Temperley-Craig calculations, detonation probably not reaching the charge surface everywhere at the same instant. The theoretical curves of other workers in this field are given in figure 6 together with the experimental curve obtained by U.S. experimenters for ranges greater than about 10 charge radii (Kirkwood et al. 1943; Penney 1940; Penney & Dasgupta 1942; Coles et al. 1946).
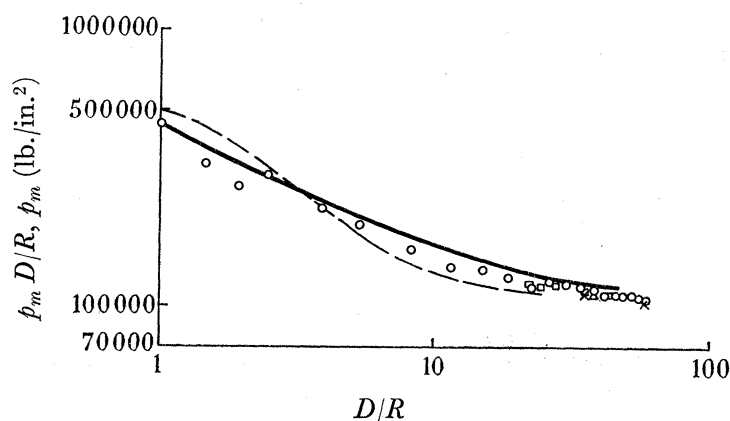


FIGURE 5. Maximum pressure $\times D/R$ against $D/R$, for spherical P.E. charges.

○ $\frac{1}{4}$ lb. P.E. 3A, $\frac{1}{4}$ in. dia. gauge;    □ $\frac{1}{8}$ to 1 lb. P.E. 3A, $\frac{1}{4}$ in. dia. gauge;
× $\frac{1}{4}$ lb. P.E. 2, $\frac{1}{4}$ in. dia. gauge;    △ 1 lb. P.E. 2, $\frac{1}{2}$ in. dia. gauge.

—— Kirkwood-Brinkley (1944) (spherical T.N.T. charge).
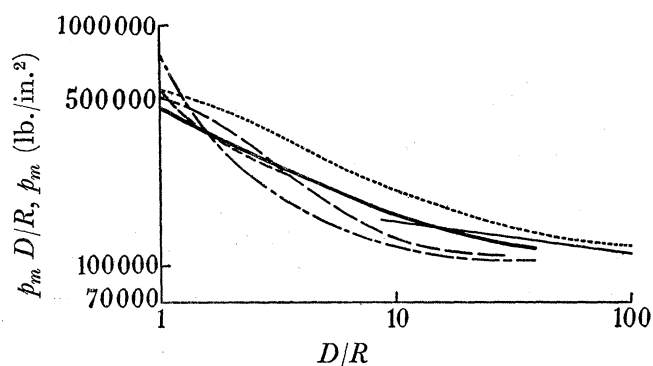— — Temperley-Craig (1945) (spherical T.N.T. charge).



FIGURE 6. Maximum pressure $\times D/R$ against $D/R$;
theoretical curves for spherical T.N.T. charges.

—— U.S. NavOrd 103 (1946).    - - - - Penney (1940).
— — Temperley-Craig (1945).    —·—· Penney-Dasgupta (1942).
..... Kirkwood-Bethe (1943).    —— Kirkwood-Brinkley (1944).

164                               A. H. BEBB

Figures 7 and 8 show similar peak pressures and $p_m D/R$ data for the approximately cylindrical $1\frac{1}{4}$ lb. T.N.T. explosive for ranges extending from 100 to 4 charge radii, together with the Temperley-Craig and Kirkwood-Brinkley curves for spherical T.N.T. explosives. The experimental deviation from the acoustic law is still apparent, but certainly not to the marked degree obtained for spherical charges, and to the degree expected from theory for
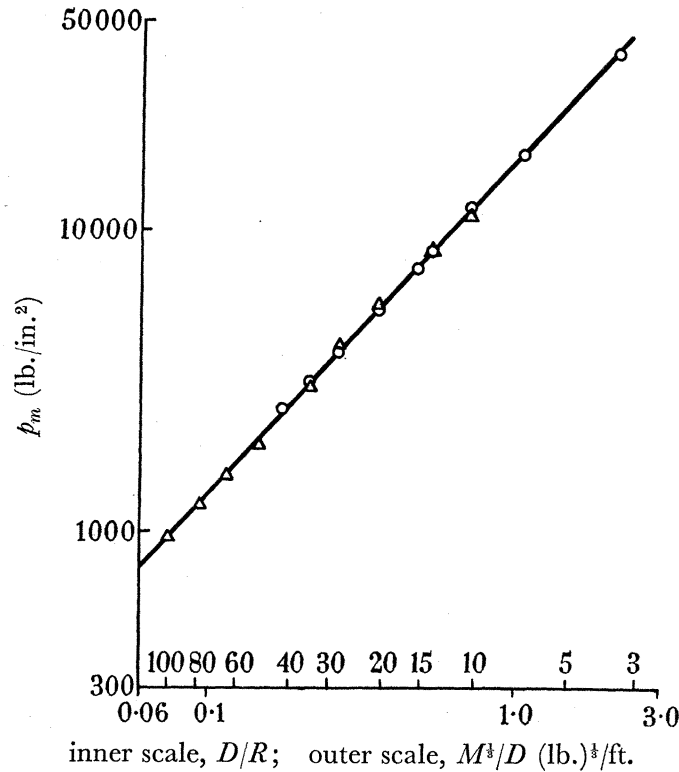


inner scale, $D/R$;    outer scale, $M^{\frac{1}{3}}/D$ (lb.)$^{\frac{1}{3}}$/ft.

FIGURE 7.  Maximum pressure against $M^{\frac{1}{3}}/D$ and $D/R$, for (approximately) cylindrical T.N.T. charges.

○ $1\frac{1}{4}$ lb. T.N.T., $\frac{1}{4}$ in. dia. gauge;    △ $1\frac{1}{4}$ lb. T.N.T., $\frac{1}{2}$ in. dia. gauge.
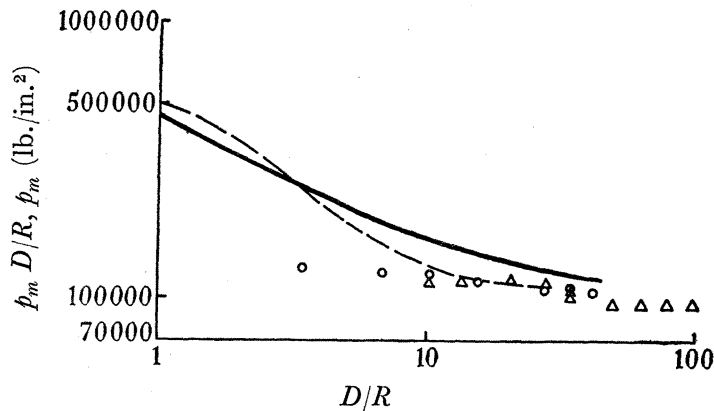$$p_m = 16{,}500 \ (M^{\frac{1}{3}}/D)^{1\cdot10}$$



FIGURE 8.  Maximum pressure $\times D/R$ against $D/R$, for (approximately) cylindrical T.N.T. charges.

○ $1\frac{1}{4}$ lb. T.N.T., $\frac{1}{4}$ in. dia. gauge;    △ $1\frac{1}{4}$ lb. T.N.T., $\frac{1}{2}$ in. dia. gauge.
———— Kirkwood-Brinkley (1944) (spherical T.N.T. charge).
— — Temperley-Craig (1945) (spherical T.N.T. charge).

spherical T.N.T. charges. This, it is suggested at near ranges, is due to (a) the less accurate method of mounting gauges and charges when the T.N.T. records were obtained, (b) the fact that the calculated charge radius 1·745 in. (R) being greater than the actual charge radius of the cylindrical block 1·225 in., the nearest point of the charge to the gauge is greater than if the charge were a sphere, (c) directional effects from a finite cylindrical block of explosive, and (d) detonation not reaching the charge surface at the same instant.

### Shock-wave time-constant

The experimental time-constant plots for spherical P.E. and cylindrical T.N.T. explosives are shown on figures 9 and 10. The theoretical derived curves of Kirkwood & Bethe (1943) for spherical T.N.T. charges are superimposed on both these figures for comparison, and the agreement is certainly fairly satisfactory considering that the Kirkwood-Bethe theory (figure 6) gives too high values for peak pressures.
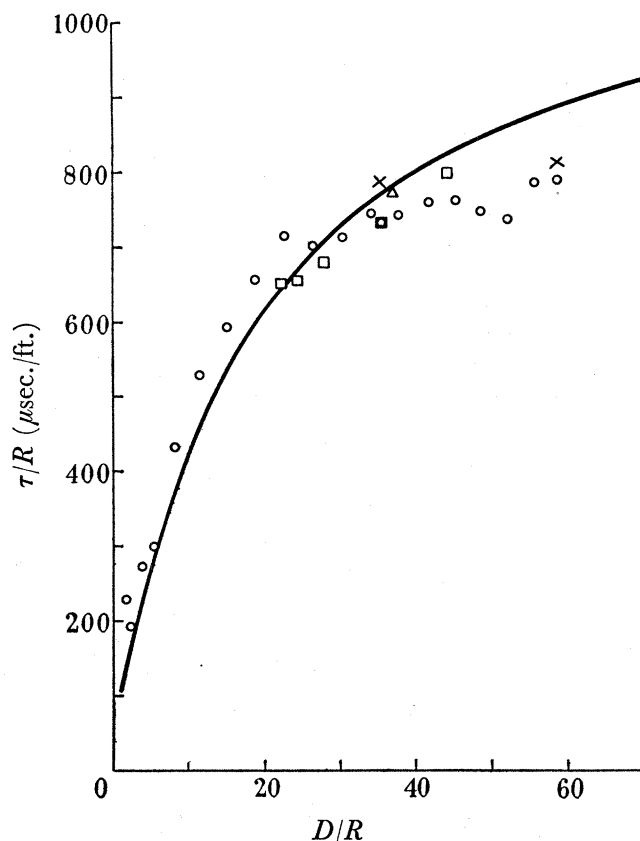


FIGURE 9. Time-constant/$R$ against $D/R$, for spherical P.E. charges.

○ $\frac{1}{4}$ lb. P.E. 3A, $\frac{1}{4}$ in. dia. gauge;      × $\frac{1}{4}$ lb. P.E. 2, $\frac{1}{4}$ in. dia. gauge;
□ $\frac{1}{8}$ to 1 lb. P.E. 3A, $\frac{1}{4}$ in. dia. gauge;   △ 1 lb. P.E. 2, $\frac{1}{2}$ in. dia. gauge.
—— Kirkwood-Bethe (1943) (spherical T.N.T. charge).

### Shock-wave velocity

The manner in which the *mean* shock-wave velocity between two points varies with the *instantaneous* peak pressure midway between the points is shown in figure 11. On this graph is also plotted the theoretical curve giving the *instantaneous* velocities corresponding to peak pressures. Bearing in mind this difference in presentation, it is considered that the experimental results tend to confirm theory.
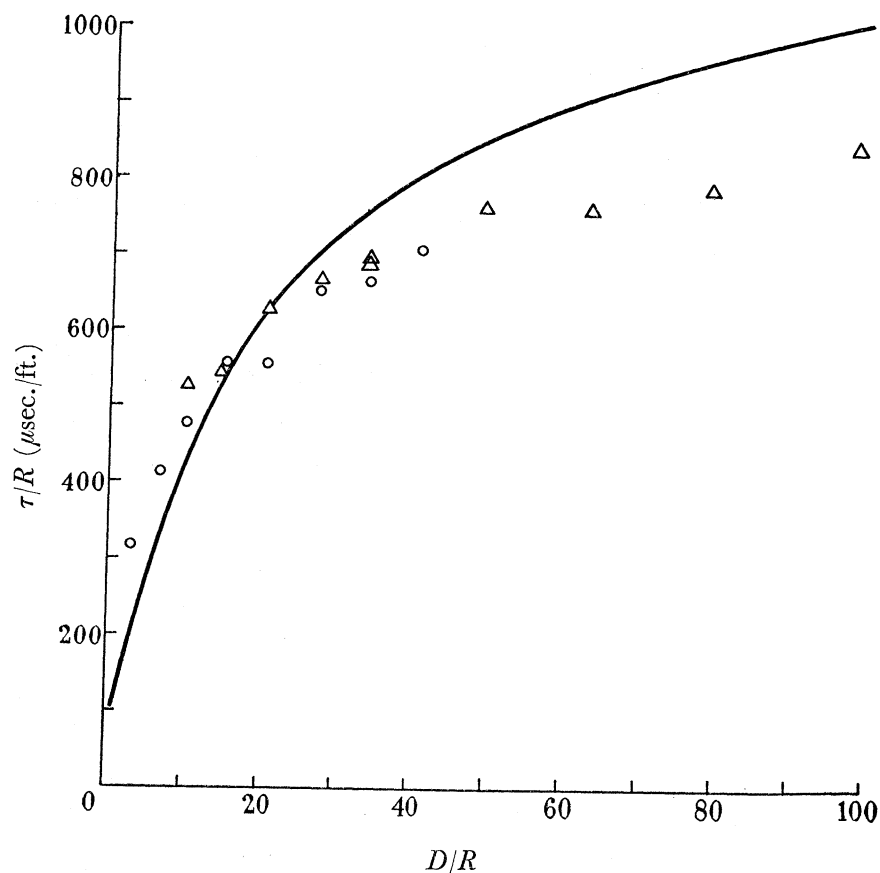
FIGURE 10. Time-constant/$R$ against $D/R$, for (approximately) cylindrical T.N.T. charges.
○ $1\frac{1}{4}$ lb. T.N.T., $\frac{1}{4}$ in. dia. gauge;    △ $1\frac{1}{4}$ lb. T.N.T., $\frac{1}{2}$ in. dia. gauge.
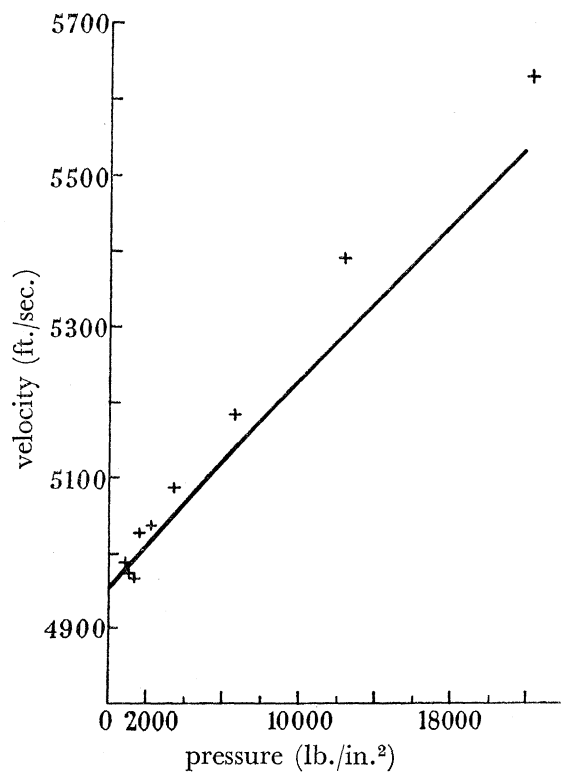—— Kirkwood-Bethe (1943) (spherical T.N.T. charge).



FIGURE 11. Shock-wave velocity against maximum pressure.
—— theoretical; + experimental (mean velocities measured over a base line of 1 ft.).

### Shock-wave impulse

Figures 12 and 13 show how impulse of unit area varies with range for spherical P.E. and T.N.T. explosives respectively. For both types of explosives there is a tendency at a range around 13 charge radii for the impulse curves to begin decreasing in slope. Since the impulse is a measure of the area of the pressure-time curve integrated in this work from zero time to $10\tau$, and the shock-wave profile becomes very thin at near ranges, i.e. $\tau$ rapidly falling, it would appear that some kind of area or impulse reduction might be expected in spite of
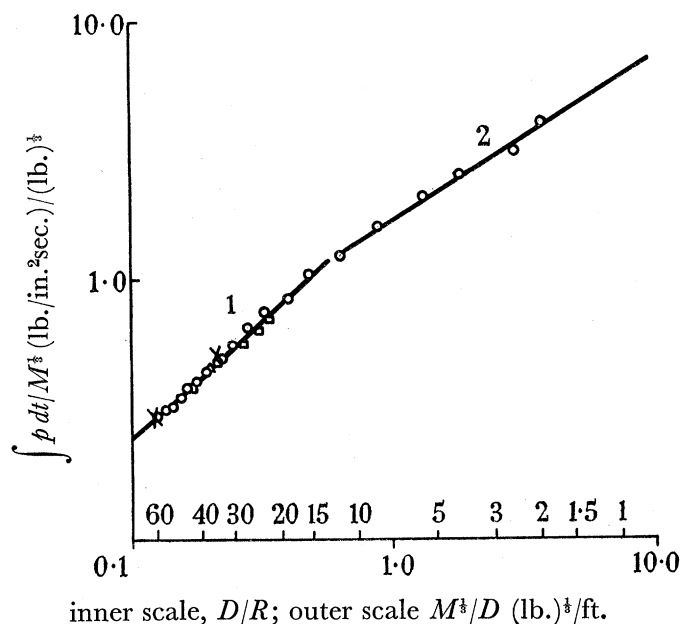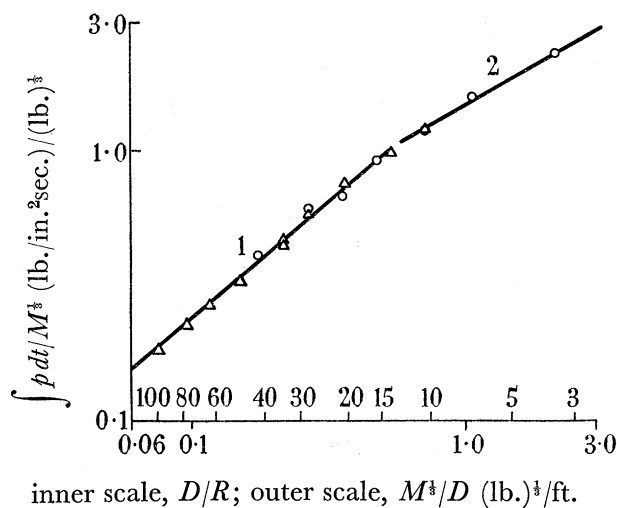


inner scale, $D/R$; outer scale $M^{\frac{1}{3}}/D$ (lb.)$^{\frac{1}{3}}$/ft.

FIGURE 12

inner scale, $D/R$; outer scale, $M^{\frac{1}{3}}/D$ (lb.)$^{\frac{1}{3}}$/ft.

FIGURE 13

FIGURE 12. Impulse of unit area/$M^{\frac{1}{3}}$ against $M^{\frac{1}{3}}/D$ and $D/R$, for spherical P.E. charges.

Curve 1, $\int p\,dt = 1\cdot 93 M^{0\cdot 63}/D^{0\cdot 90}$; curve 2, $\int p\,dt = 1\cdot 64 M^{0\cdot 54}/D^{0\cdot 62}$.

○ $\frac{1}{4}$ lb. P.E. 3A, $\frac{1}{4}$ in. dia. gauge;　　× $\frac{1}{4}$ lb. P.E. 2, $\frac{1}{4}$ in. dia. gauge;
□ $\frac{1}{8}$ to 1 lb. P.E. 3A, $\frac{1}{4}$ in. dia. gauge;　△ 1 lb. P.E. 2, $\frac{1}{2}$ in. dia. gauge.

FIGURE 13. Impulse of unit area/$M^{\frac{1}{3}}$ against $M^{\frac{1}{3}}/D$ and $D/R$, for (approximately) cylindrical T.N.T. charges.

Curve 1, $\int p\,dt = 1\cdot 77 M^{0\cdot 62}/D^{0\cdot 87}$; curve 2, $\int p\,dt = 1\cdot 49 M^{0\cdot 53}/D^{0\cdot 58}$.

○ $1\frac{1}{4}$ lb. T.N.T., $\frac{1}{4}$ in. dia. gauge;　△ $1\frac{1}{4}$ lb. T.N.T., $\frac{1}{2}$ in. dia. gauge.

observed enhanced peak pressures at close ranges. Furthermore, at close ranges of 5 charge radii and less, there is no readable positive pressure even at $10\tau$, and therefore this would contribute to a further decrease in impulse. At still closer ranges, the bubble surface would tend partially to envelop the gauge.

### Primary and afterflow energy

The variation of primary shock-wave or irreversible energy-flux density with range for spherical P.E. and cylindrical T.N.T. charges is shown in figures 14 and 15 respectively. A single line suffices to fit the P.E. results. As the primary energy-flux density is proportional

168 A. H. BEBB

to the squares of the pressures, most of it is contained in the front portion of the pressure-time curve, and therefore the effect of diminishing time-constant with range would not be expected to be significant. But with the T.N.T. results, since the pressures at short ranges are less than anticipated, some slope decrease in the energy-range curve could be expected.
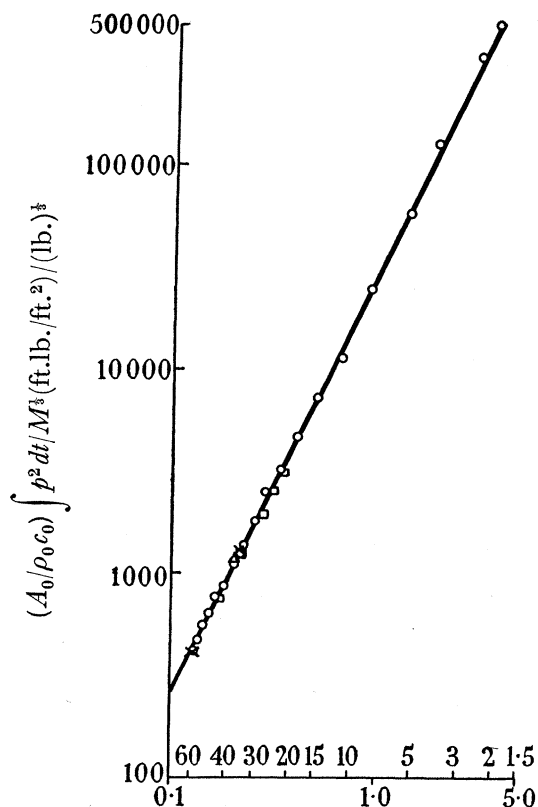


inner scale, $D/R$; outer scale, $M^{\frac{1}{3}}/D$ (lb.)$^{\frac{1}{3}}$/ft.   inner scale, $D/R$; outer scale, $M^{\frac{1}{3}}/D$ (lb.)$^{\frac{1}{3}}$/ft.
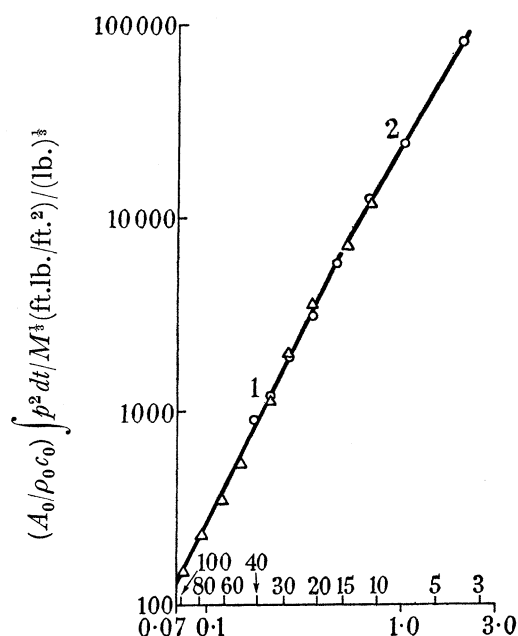
FIGURE 14                                    FIGURE 15

FIGURE 14. Primary energy-flux per unit area/$M^{\frac{1}{3}}$ against $M^{\frac{1}{3}}/D$ and $D/R$, for spherical P.E. charges.

$$(A_0/\rho_0 c_0)\int p^2\,dt = 32{,}100 M^{1\cdot03}/D^{2\cdot08}.$$

○ $\frac{1}{4}$ lb. P.E. 3A, $\frac{1}{4}$ in. dia. gauge;       × $\frac{1}{4}$ lb. P.E. 2, $\frac{1}{4}$ in. dia. gauge;
□ $\frac{1}{8}$ to 1 lb. P.E. 3A, $\frac{1}{4}$ in. dia. gauge;   △ 1 lb. P.E. 2, $\frac{1}{2}$ in. dia. gauge.
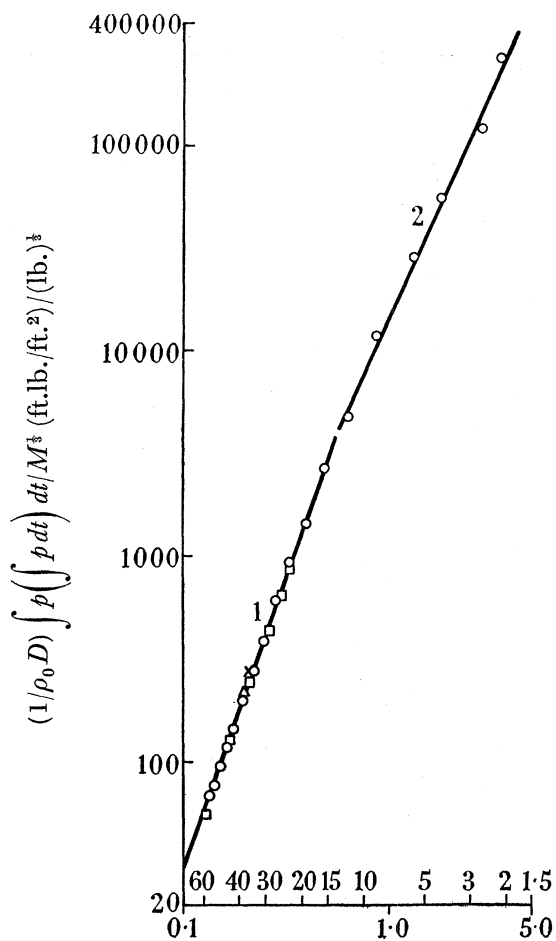
FIGURE 15. Primary energy-flux per unit area/$M^{\frac{1}{3}}$ against $M^{\frac{1}{3}}/D$, and $D/R$, for (approximately) cylindrical T.N.T. charges.

Curve 1, $(A_0/\rho_0 c_0)\int p^2\,dt = 25{,}200 M^{1\cdot00}/D^{1\cdot99}$; curve 2, $= 20{,}800 M^{0\cdot90}/D^{1\cdot70}$.

○ $1\frac{1}{4}$ lb. T.N.T., $\frac{1}{4}$ in. dia. gauge;   △ $1\frac{1}{4}$ lb. T.N.T., $\frac{1}{2}$ in. dia. gauge.

The manner in which the reversible or afterflow energy-flux density associated with explosives P.E. and T.N.T. varies with range is illustrated in figures 16 and 17. The decrease in slope at near ranges is expected for similar reasons to that already given for evaluation of impulse, since this energy term is proportional to the square of the impulse.

The significant feature to note about the afterflow energy curves is the magnitude of this energy-flux density at close ranges to the charge. This is of the same order as the primary shock-wave energy-flux density.



inner scale, $D/R$; outer scale, $M^{\frac{1}{3}}/D$ (lb.)$^{\frac{1}{3}}$/ft.  inner scale, $D/R$; outer scale, $M^{\frac{1}{3}}/D$ (lb.)$^{\frac{1}{3}}$/ft.
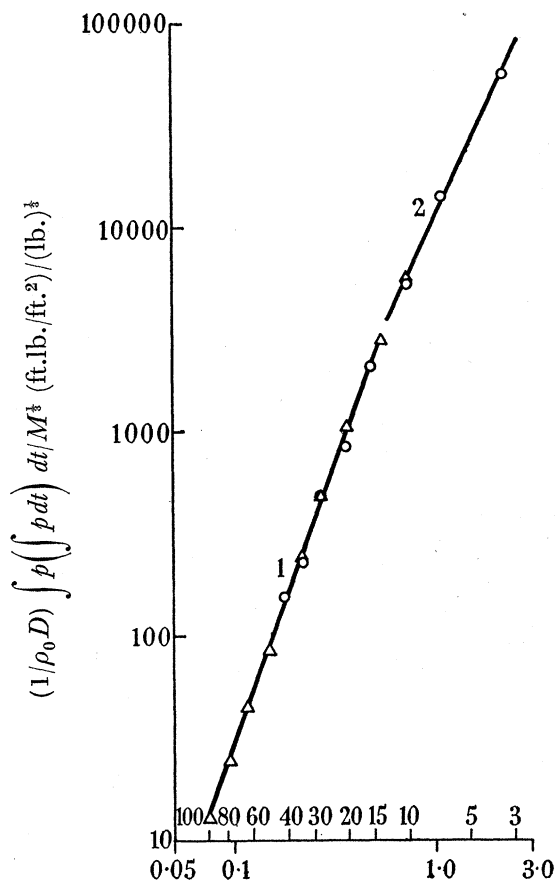
FIGURE 16  FIGURE 17

FIGURE 16. Afterflow energy-flux per unit area/$M^{\frac{1}{3}}$ against $M^{\frac{1}{3}}/D$ and $D/R$, for spherical P.E. charges.

Curve 1, $(1/\rho_0 D) \int p \left( \int p \, dt \right) dt = 19{,}000 M^{1\cdot26}/D^{2\cdot79}$; curve 2, $= 13{,}500 M^{1\cdot05}/D^{2\cdot15}$.

○ $\frac{1}{4}$ lb. P.E. 3A, $\frac{1}{4}$ in. dia. gauge;  × $\frac{1}{4}$ lb. P.E. 2, $\frac{1}{4}$ in. dia. gauge;
□ $\frac{1}{8}$ to 1 lb. P.E. 3A, $\frac{1}{4}$ in. dia. gauge;  △ 1 lb. P.E. 2, $\frac{1}{2}$ in. dia. gauge.

FIGURE 17. Afterflow energy-flux per unit area/$M^{\frac{1}{3}}$ against $M^{\frac{1}{3}}/D$ and $D/R$, for (approximately) cylindrical T.N.T. charges.

Curve 1, $(1/\rho_0 D) \int p \left( \int p \, dt \right) dt = 16{,}300 M^{1\cdot25}/D^{2\cdot74}$; curve 2, $= 11{,}400 M^{1\cdot05}/D^{2\cdot15}$.

○ $1\frac{1}{4}$ lb. T.N.T., $\frac{1}{4}$ in. dia. gauge;  △ $1\frac{1}{4}$ lb. T.N.T., $\frac{1}{2}$ in. dia. gauge.

170 A. H. BEBB

*Formulae*

The complete empirical formulae derived from this work are given in table 1.

TABLE 1

| charge ... ... ... | spherical P.E. | |
|---|---|---|
| $D/R$ between ... ... | 60 and 13 | 13 and 1 |
| maximum pressure, $p_m$ (lb./in.$^2$) | $19{,}400(M^{\frac{1}{3}}/D)^{1.15}$ | $22{,}400(M^{\frac{1}{3}}/D)^{1.45}$ |
| impulse of unit area, $\int p\,dt$ (lb./in.$^2$sec.) | $1.93M^{0.63}/D^{0.90}$ | $1.64M^{0.54}/D^{0.62}$ |
| primary energy-flux per unit area $(A_0/\rho_0 c_0)\int p^2\,dt$ (ft.lb./sq.ft. of wave front) | $32{,}100M^{1.03}/D^{2.08}$ | $32{,}100M^{1.03}/D^{2.08}$ |
| afterflow energy-flux per unit area $(1/\rho_0 D)\int p\left(\int p\,dt\right)dt$ (ft.lb./sq.ft. of wave front) | $19{,}000M^{1.26}/D^{2.79}$ | $13{,}500M^{1.05}/D^{2.15}$ |
| charge ... ... ... | cylindrical T.N.T. | |
| $D/R$ between ... ... | 100 and 13 | 13 and 4 |
| maximum pressure, $p_m$ (lb./in.$^2$) | $16{,}500(M^{\frac{1}{3}}/D)^{1.10}$ | $16{,}500(M^{\frac{1}{3}}/D)^{1.10}$ |
| impulse of unit area, $\int p\,dt$ (lb./in.$^2$sec.) | $1.77M^{0.62}/D^{0.87}$ | $1.49M^{0.53}/D^{0.58}$ |
| primary energy-flux per unit area $(A_0/\rho_0 c_0)\int p^2\,dt$ (ft.lb./sq.ft. of wave front) | $25{,}200M^{1.00}/D^{1.99}$ | $20{,}800M^{0.90}/D^{1.70}$ |
| afterflow energy-flux per unit area $(1/\rho_0 D)\int p\left(\int p\,dt\right)dt$ (ft.lb./sq.ft. of wave front) | $16{,}300M^{1.25}/D^{2.74}$ | $11{,}400M^{1.05}/D^{2.15}$ |

*Energy distribution*

The table given in appendix 4 shows that at short ranges from an explosive charge fired under water, the reversible energy-flux density associated with the velocity imparted to the water is of considerable magnitude. The primary and afterflow energy-flux densities are about equal at a range of 4 charge radii. Furthermore, whilst the primary shock-wave energy accounts for about 23 % of the available chemical energy in the explosive, about 24 % is available as reversible energy for subsequent bubble pulses.

The results given in this paper have been obtained through the co-operation of the following: Messrs P. Savic, R. V. Bundy, D. R. J. Wallace, D. George and J. L. McKeeman.

For permission to publish the paper, the author wishes to express his indebtedness to the Admiralty.

APPENDIX 1. PRIMARY SHOCK-WAVE ENERGY-FLUX DENSITY:
CORRECTION FOR FINITE AMPLITUDE WAVES

The standard expression for energy-flux density of acoustic waves of small amplitude needs modification to deal with steep-fronted explosive shock-waves. This modification is based on the theoretical work of Kirkwood & Bethe (1942), Cole (1948), and in particular on Arons & Yennie's (1947) derivations.

For acoustic waves of infinitesimal amplitudes, the energy-flux density is given by

$$E_f = (1/\rho_0 c_0) \int p^2 \, dt. \tag{A 1·1}$$

To consider finite amplitude waves, equations derived by Rankine and Hugoniot for regions behind and ahead of a discontinuous shock-wave front must be employed. The corrected equation for energy-flux density, valid at the shock front, becomes

$$E_f = (1/\rho_0) \int p^2/(U - p/\rho_0 U) \, dt, \tag{A 1·2}$$

where $U$ is the shock-front velocity.

For pressures from zero up to 40,000 lb./in.² which apply to the T.N.T. results of this paper, it is valid to assume the following relationship between shock-wave velocity $U$ and pressure $p$:

$$U = c_0(1 + \alpha_0 p). \tag{A 1·3}$$

Substituting for $U$ in (A 1·2) and simplifying,

$$E_f \doteqdot (1/\rho_0 c_0) \int \{p^2 + (1/\rho_0 c_0^2 - \alpha_0) p^3\} \, dt. \tag{A 1·4}$$

Assuming now that the shock-wave pressure-time equation is given by

$$p = p_m \exp(-t/\tau), \tag{A 1·5}$$

then

$$\int_0^\infty p^2 \, dt = \tfrac{1}{2} p_m^2 \tau \tag{A 1·6}$$

and

$$\int_0^\infty p^3 \, dt = \tfrac{2}{3} p_m \int_0^\infty p^2 \, dt. \tag{A 1·7}$$

Substituting for (A 1·6) and (A 1·7) in (A 1·4), then

$$E_f \doteqdot (1/\rho_0 c_0) \left\{1 - \tfrac{2}{3}(\alpha_0 - 1/\rho_0 c_0^2) p_m\right\} \int p^2 \, dt \tag{A 1·8}$$

or

$$E_f = (A_0/\rho_0 c_0) \int p^2 \, dt, \tag{A 1·9}$$

where

$$A_0 = 1 - \tfrac{2}{3}(\alpha_0 - 1/\rho_0 c_0^2) p_m. \tag{A 1·10}$$

For pressures from zero up to 140,000 lb./in.² which apply to the P.E. results, a more correct relation between shock-wave velocity than (A 1·3) is required. This is

$$U = c_0(1 + \alpha p + \beta p^2). \tag{A 1·11}$$

By a similar algebraic process, it may be deduced that equation (A 1·9) still holds, provided

$$A_0 = 1 - \tfrac{2}{3}(\alpha - 1/\rho_0 c_0^2) p_m + \tfrac{1}{2}(\alpha^2 - 3\alpha/\rho_0 c_0^2 - \beta + 1/\rho_0^2 c_0^4) p_m^2. \tag{A 1·12}$$

Before the primary or irreversible shock-wave energy-flux density expressed by (A 1·9) can be determined, the values of $A_0$ given by (A 1·10) and (A 1·12) have to be evaluated.

The experimental results obtained, showing variations of mean shock-wave velocities with pressures at a sea-water temperature of 17° C, are shown in figure 11. The mean shock-wave velocity at the lowest recorded pressure (884 lb./in.²) is 4981 ft./sec., which is somewhat

higher, as expected, than the quoted sound-wave value (at zero pressure) of 4954 ft./sec. at 17° C given in Matthews's tables (1939). This gives the basis for quoting Matthews's zero-pressure sound-wave velocities at 3·0 and 9·2° C respectively, the mean sea-water temperatures at which the pressure-time pulses for T.N.T. and P.E. respectively were recorded. Starting from these substantiated zero-pressure velocities, theoretical shock-wave velocity-pressure columns were derived from U.S. reports (Arons & Halverson 1944, 1946).

Using equation (A 1·3), with $c_0 = 4786$ ft./sec. at 3° C, the method of least squares (Whittaker & Robinson 1942) was employed to determine the most plausible value of $\alpha_0$ within the pressure range 0 to 40,000 lb./in.². Again, from equation (A 1·11), with $c_0 = 4868$ ft./sec. at 9·2° C, the most plausible values for $\alpha$ and $\beta$ were similarly determined within the pressure range 0 to 140,000 lb./in.².

For the T.N.T. explosive series, the energy-flux density then becomes

$$E_f = (1 - 1·49 \times 10^{-6} p_m)/\rho_0 c_0 \int p^2 \, dt. \tag{A 1·13}$$

Similarly for the P.E. explosive series, the energy-flux density may be shown to be

$$E_f = \{1 - (1·63 \times 10^{-6} p_m - 0·36 \times 10^{-12} p_m^2)\}/\rho_0 c_0 \int p^2 \, dt. \tag{A 1·14}$$

These two expressions have been used to determine the primary or irreversible energy in shock-waves of finite amplitudes.

### APPENDIX 2. ENERGY-FLUX DENSITY AND TOTAL ENERGY FROM AN UNDER-WATER EXPLOSION, USING ACOUSTIC APPROXIMATIONS

#### BY P. SAVIC, PH.D.

If the pressure $p_D$ is measured at a distance $D$ from the explosive charge, then the work done by the water on a spherical surface of radius $D$ is

$$W = (4\pi D^2) \int_0^t p_D v \, dt, \tag{A 2·1}$$

where $v$ is the velocity of water at $D$.

Since the velocity potential $\phi$ of a spherical wave is given by

$$\phi = f(t - D/c)/D, \tag{A 2·2}$$

where $f$ is an arbitrary function and $c$ is the velocity of sound, hence

$$v = -\partial\phi/\partial D$$
$$= f(t - D/c)/D^2 + (1/cD) f'(t - D/c). \tag{A 2·3}$$

But from Bernoulli's equation

$$p_D = \rho \, \partial\phi/\partial t, \tag{A 2·4}$$

where $\rho$ is the density of water (terms in $v^2$ being neglected).

From (A 2·3) and (A 2·4), it follows that

$$v = (1/\rho D) \int_0^t p_D \, dt + (1/\rho c) p_D. \tag{A 2·5}$$

Hence, substituting in (A 2·1) for $v$,

$$W = (4\pi D^2)\left\{(1/\rho c)\int_0^t p_D^2\,dt + (1/\rho D)\int_0^t p_D\int_0^{t'} p_D\,dt\,dt'\right\}. \qquad (A\,2\cdot6)$$

It will be seen from its definition that $W$ is also the energy-flux in time $t$ through a spherical surface of radius $D$.

The energy-flux becomes equal to the total energy in the water only if at time $t$ the surface of the reference sphere is coincident with the surface of the bubble. At this point all the energy except the energy remaining inside the bubble gases has passed through the surface of the reference sphere.

Denoting the radius of the bubble at time $t$ by $a$, the total energy in the water is

$$E = (4\pi a^2)\left\{(1/\rho c)\int_0^t p_a^2\,dt + (1/\rho a)\int_0^t p_a\int_0^{t'} p_a\,dt\,dt'\right\}, \qquad (A\,2\cdot7)$$

where $p_a$ is the pressure as measured at a distance $a$ from the charge.

But assuming $p_a$ and $p_D$ to be related by

$$ap_{a\text{ at time }t} = Dp_{D\text{ at time }(t+D/\bar{U})}, \qquad (A\,2\cdot8)$$

then on substituting in (A 2·7),

$$E = (4\pi D^2)\left\{(1/\rho c)\int_0^{t+D/\bar{U}} p_D^2\,dt + (D/a\,.\,1/\rho D)\int_0^{t+D/\bar{U}} p_D\int_0^{t'} p_D\,dt\,dt'\right\}, \qquad (A\,2\cdot9)$$

where $a$ is the radius of the bubble at time $(t+D/\bar{U})$ after the explosion, $\bar{U}$ being the mean propagation velocity of the shock-wave.

It is seen that the second or afterflow term in (A 2·9) is different from the corresponding term in (A 2·6). This is due to the fact that whereas an acoustic shock-wave travels through the water without any further expenditure of energy, the incompressive afterflow depends for its transport on the actual movement of the whole mass of water.

### Appendix 3. Comparison of afterflow and primary energy-flux densities

The afterflow energy-flux density is given by

$$\begin{aligned}
E_f' &= (1/\rho_0 D)\int p\left(\int p\,dt\right)dt \\
&= (1/2\rho_0 D)\left(\int p\,dt\right)^2 \\
&= I^2/2\rho_0 D \\
&= k'M^{\frac{4}{3}}/D^3, \qquad (A\,3\cdot1)
\end{aligned}$$

if it is assumed that the impulse of unit area $I$ is proportional to $M^{\frac{2}{3}}/D$.

The primary energy-flux density is given by

$$\begin{aligned}
E_f &= (1/\rho_0 c_0)\int p^2\,dt \\
&= kM/D^2. \qquad (A\,3\cdot2)
\end{aligned}$$

174 A. H. BEBB

Hence $$E_f'/E_f = K(D/R)^{-1},$$ (A 3·3)

where $K$ is a constant and $R$ the explosive charge radius. Whilst the above formulae are not rigorously correct, equation (A 3·3) indicates the relative importance of the afterflow energy-flux density in the vicinity of an under-water explosion.

It must be realized, however, that the total afterflow energy in the water is independent of $D/R$.

### Appendix 4. Total energy from an under-water explosion

The total energy in the water from an under-water explosion is given by

$$(4\pi D^2 \times \text{primary energy-flux density}) + (4\pi D^2 \times D/a \times \text{afterflow energy-flux density}),$$

where $a$ is the radius of the explosion bubble at the limit of integration of the pressure-time pulse. In the early stages of bubble formation, theory shows that there is considerable uncertainty in this region, but an extrapolated value for the explosion bubble radius was determined from the theoretical work (Taylor 1942; Comrie & Hartley 1942). As the formulae for primary and afterflow energy-flux densities were determined empirically, the total primary and afterflow energies are calculable. The primary and afterflow energy-flux density formulae for long ranges were used for this calculation.

The following table has been derived:

| explosive | $D/R$ | ratio of the afterflow energy flux per sq.ft. of wave front to the primary energy flux per sq.ft. of wave front | primary energy as a fraction of the total chemical energy | afterflow energy as a fraction of the total chemical energy |
|---|---|---|---|---|
| P.E. (spherical) | 50 | 0·15 | 0·20 | 0·23 |
|  | 15 | 0·36 | 0·22 | 0·21 |
|  | 5 | 0·78 | 0·24 | 0·21 |
|  | 1 | 2·46 | 0·27 | 0·24 |
| T.N.T. (cylindrical) | 50 | 0·15 | 0·23 | 0·29 |
|  | 15 | 0·38 | 0·23 | 0·25 |
|  | 5 | 0·87 | 0·23 | 0·23 |

(The total chemical energy available in T.N.T. has been taken as 1000 cal./g., i.e. $1·41 \times 10^6$ ft.lb./lb.; and as $1·76$ ft.lb./lb. for P.E. on the basis of the present work.)

### References

Symbols NavOrd, N.R.L. O.S.R.D., and T.M.B. refer to United States reports:

NavOrd = Naval Ordnance Laboratory.
N.R.L. = Naval Research Laboratory.
O.S.R.D. = Office of Scientific Research and Development.
T.M.B. = Taylor Model Basin.

Arons, A. B. & Halverson, R. R. 1944 O.S.R.D. 4406.
Arons, A. B. & Halverson, R. R. 1946 O.S.R.D. 6577.
Arons, A. B. & Smith, P. F. 1946 NavOrd 104.
Arons, A. B. & Yennie, D. R. 1947 NavOrd 406.
Bebb, A. H. & Bundy, R. V. 1945 Undex 131, 199. Admiralty.

Bebb, A. H., Wallace, D. R. J., Pringle, D. H. & Bundy, R. V. 1946 Undex 195. Admiralty.

Bebb, A. H., Wallace, D. R. J., Taylor, D. W., Bundy, R. V. & Hendry, G. 1947 Undex 215. Admiralty.

Bryant, A. R. 1945 Undex 140. Admiralty.

Cole, R. H. 1944 O.S.R.D. 4561.

Cole, R. H. 1948 *Underwater explosions*. New Jersey: Princeton University Press.

Cole, R. H. & Coles, J. S. 1947 *Phys. Rev.* **71** (2).

Coles, J. S., Christian, E. A., Slifko, J. P., Niffenegger, C. R. & Rogers, M. A. 1946 NavOrd 103.

Comrie, L. J. & Hartley, H. O. 1942 SW 26. Scientific Computing Service.

Greenfield, M. A. & Shapiro, M. M. 1944 T.M.B. 523.

Kennard, E. H. 1941 T.M.B. 480.

Kirkwood, J. G. & Bethe, H. A. 1942 O.S.R.D. 588.

Kirkwood, J. G. & Brinkley, S. R. 1944 O.S.R.D. UE-24.

Kirkwood, J. G. & Brinkley, S. R. 1945 O.S.R.D. 4814.

Kirkwood, J. G., Brinkley, S. R. & Richardson, J. M. 1943 O.S.R.D. 2022.

Kirkwood, J. G. & Montroll, E. W. 1942 O.S.R.D. 676.

Kirkwood, J. G., Montroll, E. W. & Richardson, J. M. 1942 O.S.R.D. 1030.

Kirkwood, J. G. & Richardson, J. M. 1942 O.S.R.D. 813.

Lampson, C. W. 1943 O.S.R.D. 1179.

Matthews, D. J. 1939 H.D. 282. Admiralty.

Munz, H. A. 1945 Undex 173. Admiralty.

Osborne, M. F. M. & Taylor, A. H. 1944 N.R.L. S-2305.

Osborne, M. F. M. & Taylor, A. H. 1946 *Phys. Rev.* **70** (5, 6).

O.S.R.D. 4874 1945.

Penney, W. G. 1940 RC 142. Ministry of Home Security.

Penney, W. G. & Dasgupta, H. K. 1942 RC 333. Ministry of Home Security.

Taylor, G. I. 1942 SW 19. Ministry of Home Security.

Temperley, H. N. V. & Craig, J. 1945 Undex 136. Admiralty.

Whittaker, E. T. & Robinson, G. 1942 *The calculus of observations*. London: Blackie and Son, Ltd.

Wood, A. B. & Lakey, E. H. 1924 ARL/S/12. Admiralty.

Yule, G. U. & Kendall, M. G. 1945 *An introduction to the theory of statistics*. London: Griffin and Co. Ltd.

FIGURE 1. Piezo-electric gauge before application of rubberoid wax and natural latex. Also after completion of curing process.
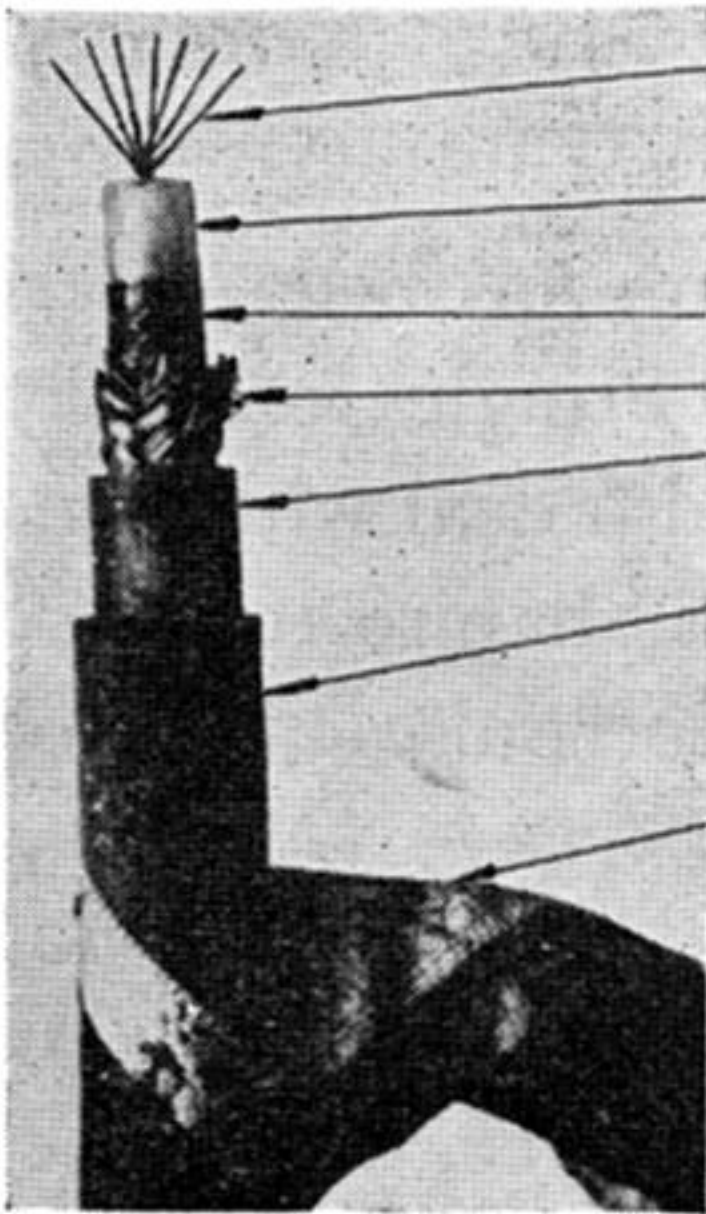
central conductors

telcothene

Aquadag or graphite braid

outer telcothene covering

tough rubber sheath

canvas tape

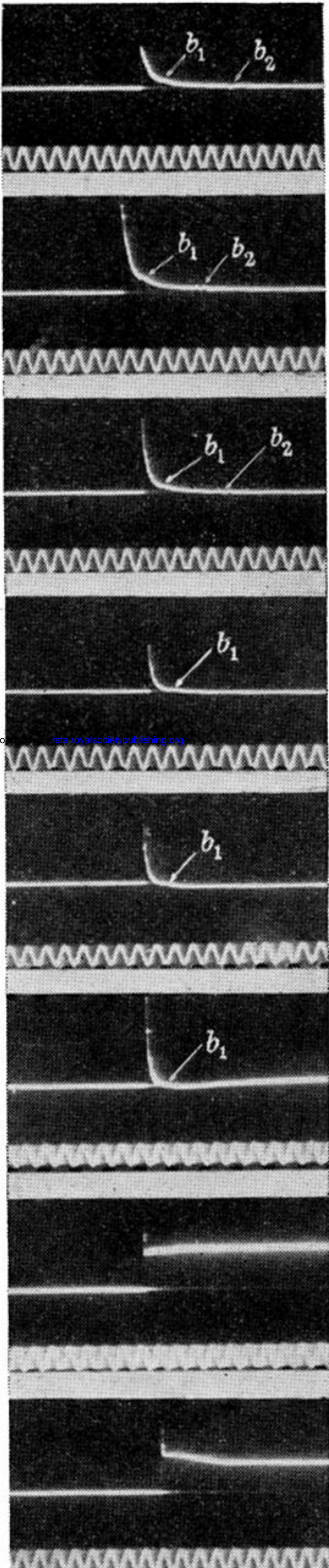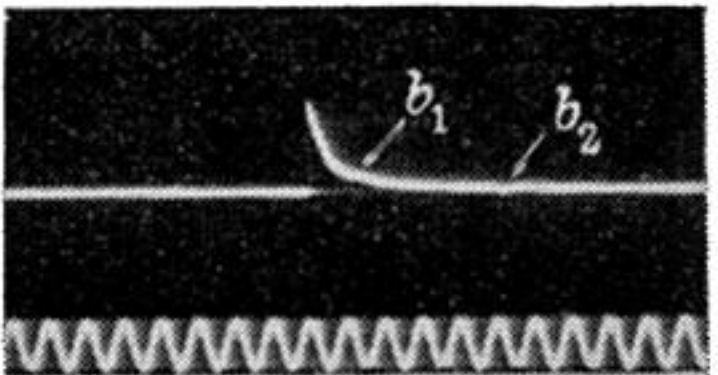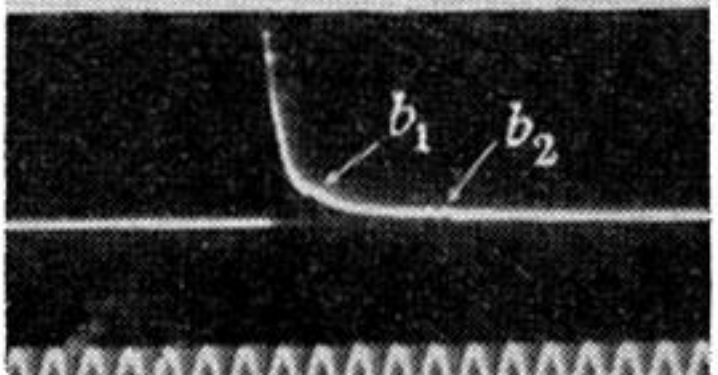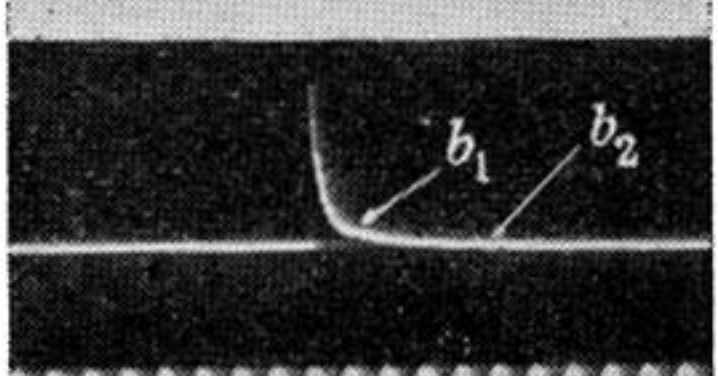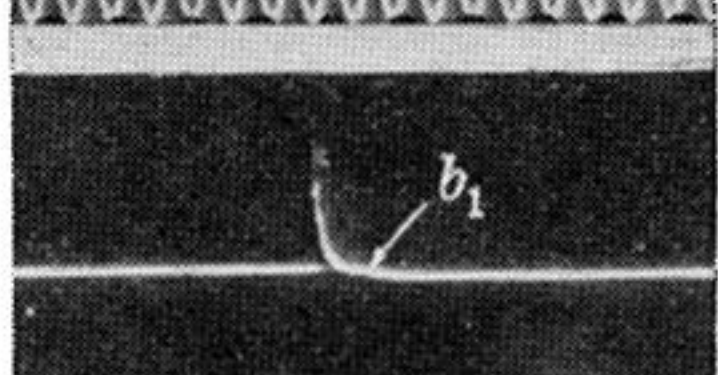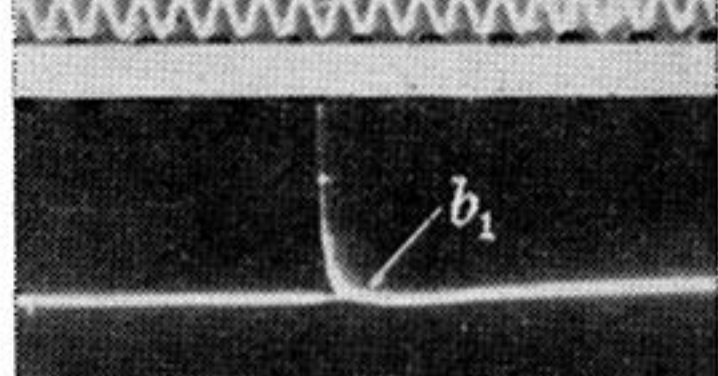FIGURE 2. Special cable for use with piezo-electric gauge.

| record | | total circuit capacity in $\mu$F | distances from charge in in. | distances/ charge radii $D/R$ | observed maximum pressures, $p_m$, in lb./in.$^2$ |
|---|---|---|---|---|---|
| 1 | | 0·02515 | 23·10 | 22·6 | 5,120 |
| 2 | | 0·02515 | 11·94 | 11·7 | 11,660 |
| 3 | | 0·09530 | 5·52 | 5·4 | 35,750 |
| 4 | | 0·2660 | 4·02 | 3·9 | 56,030 |
| 5 | | 0·3033 | 2·52 | 2·5 | 119,400 |
| 6 | | 0·3031 | 2·00 | 2·0 | 135,500 |
| 7 | | 1·003 | 1·02 | 1·0 | 450,600 |
| 8 | | 3·808 | 0·0 | 0·0 | 1,160,000 |

FIGURE 3. Typical pressure-time records from $\frac{1}{4}$ lb. P.E. 3A spherical charges with a $\frac{1}{4}$ in. diameter tourmaline gauge. (Time scale for records = 10,000 c./sec.)